High-dimensional Detection of Spatial Interference Effects

Wei Zhang
School of Mathematical Sciences, Center for Statistical Science,
Peking University, Beijing, China
Ying Yang
Center for Applied Mathematics, Fudan University, Shanghai, China,
Fang Yao*
School of Mathematical Sciences, Center for Statistical Science,
Peking University, Beijing, China

March 28, 2025

Abstract

Modeling interference effects in high-dimensional settings presents significant challenges due to the complexity of underlying dependence structures. Existing approaches often rely on explicit and homogeneous assumptions, limiting their applicability in real-world scenarios. In this paper, we introduce a novel low-rank and sparse treatment effect model that leverages high-dimensional techniques to identify interference structures without restrictive parametric assumptions. We propose an efficient profiling algorithm for estimating model coefficients and develop statistical methodologies for both global testing of interference existence and local detection of interference-affected units. Theoretical guarantees are established, including non-asymptotic error bounds for estimation and accuracy guarantees for detection based on the Jaccard index. Through numerical experiments, we demonstrate the effectiveness of our method in high-dimensional settings, highlighting its advantages in capturing complex interference patterns.

Keywords: interference detection, low-rank and sparse model, riding market

*The first two authors are co-first authors and contribute equally. Corresponding author: fyao@math.pku.edu.cn.

1 Introduction

The Interference Effect (IE) — defined as the spillover impact where treatments applied to one unit affect the outcomes of others — introduces complex interdependencies that pose significant challenges for causal identification and policy optimization in economic and business systems. This phenomenon is pervasive across various domains: social networks propagate opinions and behaviors (Goldsmith-Pinkham & Imbens 2013, Graham et al. 2010), peer effects shape corporate investment decisions (Arpino & Mattei 2016), educational outcomes are influenced by peer learning strategies (VanderWeele et al. 2013), and environmental regulations create cross-regional pollution externalities (Papadogeorgou et al. 2019*a*). A prominent contemporary manifestation of IE arises in the sharing economy, particularly in ride-hailing platforms. For instance, targeted incentive policies for specific driver cohorts can disrupt equilibrium in interconnected labor markets, influencing supply-demand ratios and dynamic pricing mechanisms. These effects may extend beyond directly treated areas, creating intricate spatial dependencies that further complicate policy evaluation.

Existing methods for modeling IE typically rely on strong structural assumptions to simplify the complexity of interference. These approaches often assume that the interference structure is known and fall into three primary categories. The first category is partial interference, which assumes interference is restricted within predefined clusters (Halloran & Struchiner 1991, 1995, Halloran 2012, Perez-Heydrich et al. 2014, Barkley et al. 2020, Papadogeorgou et al. 2019*b*). The second category is local network interference, which assumes interference effects are confined to the local network surrounding each node (Forastiere et al. 2021, Aronow & Samii 2017, Tchetgen et al. 2021, Giffin et al. 2020). The third category combines the interference structure with underlying mechanisms; for example, Munro et al. (2021), Wager & Xu (2021), and Johari et al. (2022) characterized inter-

ference using market equilibrium models, while Bojinov & Shephard (2019) assumed that the interference in time series problems follows a d-order lag structure.

Although these methods simplify inference by imposing structured assumptions, they fail to capture the heterogeneous and dynamic interference patterns commonly observed in real-world settings. In particular, spatial homogeneity assumptions are often unrealistic in the sharing economy, where interference structures vary considerably across regions. For example, in ride-hailing platforms, less active regions may experience interference primarily from nearby areas, while densely populated urban centers may exhibit complex spatial dependencies due to commuting patterns between residential and commercial districts.

In contrast to these approaches, we explore a different modeling strategy that leverages a distinct feature of the sharing economy: the presence of independent observations across time. In two-sided markets such as ride-hailing platforms and social networks, user and provider behaviors often follow cyclical patterns driven by daily routines. For example, ride-hailing platforms typically experience reduced activity during late-night hours, and online marketplaces such as Airbnb and e-commerce platforms exhibit demand fluctuations based on time-of-day and day-of-week effects. Consequently, in such environments, it is often reasonable to treat daily data as independent samples, an assumption widely adopted in recent studies (Zhang et al. 2022, Altshuler et al. 2019, Liu et al. 2019). Figure 1 further illustrates these temporal patterns in the ride-sharing market, further supporting the assumption of daily independence.

Building on this independence structure, we propose a novel spatial interference detection method that identifies interference structures in high-dimensional settings. Our method adopts a spatial grid framework where the interference effect on each unit may depend on the treatment assignments of all other units, posing a high-dimensional inference challenge. To mitigate this, we introduce a sparse interference assumption, which assumes that only a small subset of units contributes to interference for any given unit.

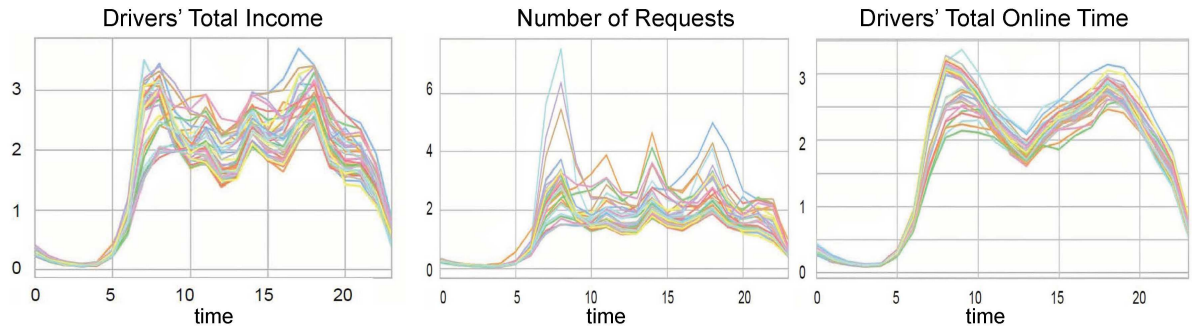

Figure 1: Business metrics from a city over 40 days, including drivers' total income, the number of requests, and drivers' total online time. Each curve represents data for a single day, with the horizontal axis corresponding to 24 hours. The values are scaled to preserve privacy.

This flexible assumption generalizes commonly used interference structures as special cases. Additionally, we incorporate spatial regularization to improve estimation efficiency. Since the spatial structure of the direct effect (DE) is typically determined by several latent-variables (Chernozhukov et al. 2021), we focus on its generalized low-rank structure in this paper. We propose a two-layer profiling algorithm to estimate the model coefficients. Based on these estimates, we conduct a global test to detect the presence of interference. If the test indicates the presence of interference, we proceed with a local detection method to identify interference-affected units. To do this, we extend high-dimensional signal detection methods, such as the binary and re-search method (Zhang et al. 2023, BiRS) and stepdown procedure (Romano & Wolf 2005), to our context, providing theoretical guarantees for both detection accuracy and statistical inference validity.

The contributions are summarized as follows.

1. This study pioneers a method for detecting interference structures at the individual unit level, providing a powerful tool for understanding complex interdependencies in economic systems. By identifying which units influence one another, our method helps avoid mis-specification of interference structures, which is crucial for accurate

policy evaluation and decision-making. Moreover, our method enables post-detection estimation of average treatment effects, offering improved insights into intervention outcomes.

2. Our approach extends traditional high-dimensional signal detection methods to the more complex sparse regression setting, which is particularly relevant in economic scenarios involving numerous covariates and unknown interference patterns. Unlike standard signal detection methods, sparse regression introduces additional complexities such as parameter tuning and model selection. To address these challenges, we propose a conditional bootstrap method that enhances the reliability of inference, ensuring robust identification of interference patterns in real-world data.

3. We provide theoretical guarantees for the proposed method. We establish non-asymptotic error bounds for the estimates and validate the inference procedure through rigorous size and power analysis. These theoretical insights ensure that our method can consistently and accurately detect interference effects under mild assumptions, making it a reliable tool for complex economic systems.

4. Our method addresses several practical challenges that commonly arise in business and economic applications. Firstly, it accommodates heterogeneous interference structures, making it adaptable to diverse settings such as geographically dispersed markets and cross-regional policy evaluations. Secondly, the low-rank and sparse constraints enhance estimation efficiency, making the method particularly effective in scenarios where interference effects are subtle or data availability is limited. Thirdly, by detecting interference patterns at the unit level, our method offers valuable insights into the underlying mechanisms through which interventions generate broader effects. This understanding can inform targeted policy design to maximize intervention impact within budget constraints — for instance, by directing incentives toward

units with high potential spillover effects.

To validate the effectiveness of our method, we conduct extensive numerical experiments and simulations that closely mimic real-world business settings. These results demonstrate the robustness and practical utility of our approach in capturing complex interference patterns and informing effective decision-making.

The rest of the paper is organized as follows. In Section 2, we introduce the sparse interference assumption under the potential outcome framework and the proposed low-rank and sparse treatment effect model. Section 3 outlines the estimation procedure as well as the methods for global testing and IE location detection. In Section 4, we derive the error bounds of the estimates and perform size and power analysis for the global test. We then describe the analysis of detection accuracy for the stepdown and BiRS algorithms. A case study for IE location detection is presented in Section 5 and comprehensive simulation studies based on China meteorological forcing dataset are conducted in Section 6. Discussions are provided in Section 7, and technical proofs of main theorems are deferred to Supplementary Material.

2 Low-rank and Sparse Treatment Effect Model

Suppose that the experimental area is partitioned into R rows and C columns of distinct, non-overlapping units. Let M_{rc} be a binary variable representing the treatment assignment to unit (r, c) and Y_{rc} the observed outcome of unit (r, c). Let M and Y be the corresponding RC-dim vectors in the whole experimental area. When SUTVA does not hold, Y_{rc} depends on M instead of M_{rc}.

2.1 Potential outcome framework and interference effect

We now use the potential outcome notations to introduce IE. Let $Y_{rc}(M)$ be the potential outcome for unit (r, c) under treatment M. As pointed out by Rubin (1986), the potential outcome is well-defined only if the following assumption holds:

Assumption 1 *(Consistency Assumption, CA) For each unit (r, c), the observed outcome satisfies $Y_{rc} = Y_{rc}(M)$.*

Let M_{-rc} be the vector of treatments for all units other than (r, c). The individual treatment effect (ITE) for unit (r, c) is defined as

$$\begin{aligned}\mathrm{ITE}_{rc} &= \mathbb{E}\left\{Y_{rc}(M_{rc}=1, M_{-rc}=1) - Y_{rc}(M_{rc}=-1, M_{-rc}=-1)\right\} \\ &= \underbrace{\mathbb{E}\left\{Y_{rc}(1,1) - Y_{rc}(-1,1)\right\}}_{\mathrm{DE}_{rc}} + \underbrace{\mathbb{E}\left\{Y_{rc}(-1,1) - Y_{rc}(-1,-1)\right\}}_{\mathrm{IE}_{rc}},\end{aligned}$$

where DE_{rc} represents DE of M_{rc} on the outcome of unit (r, c) and IE_{rc} captures IE of M_{-rc} on Y_{rc}. The population-level effects are then given by

$$\mathrm{ATE} = (RC)^{-1}\sum_{r,c}\mathrm{ITE}_{rc},\ \mathrm{DE} = (RC)^{-1}\sum_{r,c}\mathrm{DE}_{rc},\ \text{and } \mathrm{IE} = (RC)^{-1}\sum_{r,c}\mathrm{IE}_{rc}.$$

In this paper, we focus on detecting the heterogeneous interference structure. For any unit (r, c), let $\mathcal{N}_{rc} \subset \{(r', c') \neq (r, c) : 1 \leq r' \leq R, 1 \leq c' \leq C\}$ be an index subset dependent on (r, c), and let $\mathcal{N}_{-rc}$ denote all units not in $\{i\} \cup \mathcal{N}_{rc}$. We impose the following assumption.

Assumption 2 *(Sparse Interference Assumption, SIA) For each unit (r, c), there exists an index subset $\mathcal{N}_{rc}$ with cardinal $s_{rc} \ll RC$ such that for any $M_{\mathcal{N}_{-rc}}$ and $M'_{\mathcal{N}_{-rc}}$, the potential outcomes satisfy $Y_{rc}(M_{rc}, M_{\mathcal{N}_{rc}}, M_{\mathcal{N}_{-rc}}) = Y_{rc}(M_{rc}, M_{\mathcal{N}_{rc}}, M'_{\mathcal{N}_{-rc}})$.*

The smallest $\mathcal{N}_{rc}$ satisfying Assumption 2 is the interference neighbor set of interest. We are particularly interested in detecting the elements in $\mathcal{N}_{rc}$ for each unit (r, c) from the

observational data, as this can provide insights into the mechanisms underlying treatment effects. Understanding these mechanisms can inform the development of more effective strategies. Assumption 2 covers many existing assumptions commonly used in the causal inference literature to address spatial interference, including the partial IE and local network interference (Sobel 2006, Hudgens & Halloran 2008, Liu et al. 2016, Sävje et al. 2021). However, Assumption 2 allows for variation in the interference structure across space. In scenarios where prior knowledge suggests high-dimensional interference, one may refer to Leung (2022) which assumes IE decays as the distance between two units increases. This assumption differs from our sparse interference assumption. Both assumptions have their respective advantages. While the decaying interference assumption potentially accommodates high-dimensional IE, our sparse assumption allows for distant interactions. We finally introduce the classical conditional independence assumption.

Assumption 3 *(Conditional Independence Assumption, CIA) Let X_{rc} denote the state variable for unit (r, c). The treatment assignment M is independent of all the potential outcomes conditional on the state variables $\{X_{rc}\}_{r,c}$.*

This assumption, also referred to as the unconfoundedness assumption, is fundamental for the identification of causal effects from observational data. Finally, under Assumptions 1–3, the individual DE and IE can be expressed as

$$\mathrm{DE}_{rc} = \mathbb{E}_X \left\{ \mathbb{E}(Y_{rc} | M_{rc} = 1, M_{\mathcal{N}_{rc}} = 1, X) - \mathbb{E}(Y_{rc} | M_{rc} = -1, M_{\mathcal{N}_{rc}} = 1, X) \right\},$$

$$\mathrm{IE}_{rc} = \mathbb{E}_X \left\{ \mathbb{E}(Y_{rc} | M_{rc} = -1, M_{\mathcal{N}_{rc}} = 1, X) - \mathbb{E}(Y_{rc} | M_{rc} = -1, M_{\mathcal{N}_{rc}} = -1, X) \right\},$$

with ITE_{rc} and ATE derivable in a similar manner. For the remainder of this paper, we assume that Assumptions 1–3 hold.

2.2 The proposed model

We consider an experimental setting where each unit (r, c), for $1 \leq r \leq R$ and $1 \leq c \leq C$, receives a sequence of treatments over time, generating repeated measurements. Specifically, for each unit, we observe n independent observations, denoted as $(Y_{i,rc}, X_{i,rc}, M_{i,rc})$, $i = 1, \ldots, n$, where $Y_{i,rc} \in \mathbb{R}$ is the outcome, $X_{i,rc} \in \mathbb{R}^d$ is the state variable, $M_{i,rc} \in \{-1, 1\}$ is the treatment variable. Under this framework, we assume a linear outcome regression model for each unit (r, c) without imposing a predefined spatial structure as follows,

$$Y_{i,rc} = X_{i,rc}\beta_{rc} + M_{i,rc}L_{rc} + M_{i,-rc}S_{rc} + \varepsilon_{i,rc},\ i = 1, \ldots, n, \tag{1}$$

where $\beta \in \mathbb{R}^d$ is the effect of state variables, $L_{rc} \in \mathbb{R}$ is DE at (r, c), and $S_{rc} \in \mathbb{R}^{RC-1}$ is a high dimensional vector representing IE for (r, c). The sub-gaussian random errors $\varepsilon_{i,rc}$, $i = 1, \ldots, n$ are independent with mean zero and variance σ_{rc}^2.

Under model (1), Assumption 2 aligns with the classical sparse assumption in high-dimensional linear models. To see this, let $J_1(r, c)$ be the index set of nonzero elements in S_{rc}. Then there is a one-to-one correspondence between the inference neighbor set $\mathcal{N}_{rc}$ and $J_1(r, c)$. Within the potential outcome framework, it is straightforward to verify that

$$\mathrm{DE}_{rc} = 2L_{rc},\ \mathrm{IE}_{rc} = 2\sum_{j \in J_1(r,c)} S_{rc,j},\ \text{and ATE} = \frac{2}{RC}\sum_{r,c}\left\{L_{rc} + \sum_{j \in J_1(r,c)} S_{rc,j}\right\}.$$

Once the sets $\{J_1(r, c)\}_{r,c}$ are accurately identified, model (1) reduces to an ordinary linear regression model, enabling effective inference on the effects of interest. Hence the primary objective of this paper is to detect locations of IE.

Given that the estimates of S and L are correlated (both depending on treatment variables),it is crucial that the estimate of L converge at a rate faster than root-n in order to efficiently detect the interference. To achieve this, we propose incorporating spatial information, such as low-rank, smoothness, or clustered-uniform structures, to improve the estimation accuracy of L. In this paper, we specifically focus on the generalized low-rank

structure in the sense that the matrix $L = (L_{rc})_{r,c} \in \mathcal{B}_q(v_q)$, where

$$\mathcal{B}_q(v_q) = \left\{ A \in \mathbb{R}^{m_1 \times m_2} : \sum_{i=1}^{m} \theta_i^q(A) \leq v_q, m = \min\{m_1, m_2\} \right\}$$

with $\{\theta_i(A), i = 1, \ldots, m\}$ denoting the singular values of A. The set $\mathcal{B}_q(v_q)$ provides flexibility in modeling various structures. When $q = 0$, $\mathcal{B}_0(v_0)$ corresponds to the class of matrices with at most v_0 nonzero singular values. As shown in Chernozhukov et al. (2021), generalized low-rank matrix regression encompasses a wide range of latent-variable models, capable of accommodating heterogeneous treatment effects. Furthermore, the main idea can be adapted to alternative assumptions regarding DE by adjusting the penalty term accordingly. For example, similar to Luo et al. (2024), one can also adopt smoothing techniques to enhance the accuracy of DE estimation.

3 Estimation and Detection Procedures

3.1 Estimation procedure

With a little abuse of notations, we denote $Y_{rc} = (Y_{1,rc}, \ldots, Y_{n,rc})^\top$, $X_{rc} = (X_{1,rc}, \ldots, X_{n,rc})^\top$, $M_{rc} = (M_{1,rc}, \ldots, M_{n,rc})^\top$ and $M_{-rc} = (M_{1,-rc}, \ldots, M_{n,-rc})^\top$. The target function for model (1) is

$$Q(\beta, L, S) = \frac{1}{n} \sum_{r=1}^{R} \sum_{c=1}^{C} \|Y - X_{rc}\beta_{rc} - M_{rc}L_{rc} - M_{-rc}S_{rc}\|_F^2 + \lambda \|L\|_* + \sum_{r=1}^{R} \sum_{c=1}^{C} \lambda_{rc} \|S_{rc}\|_1 , \tag{2}$$

where $\|\cdot\|_F$, $\|\cdot\|_*$ and $\|\cdot\|_1$ are the Frobenius norm, nuclear norm and 1-norm, respectively. The first term represents the loss function, while the second and third terms correspond to the low-rank structure of DE and unit-wise sparse structure of IE, respectively.

We propose to use a two-layer profiling algorithm to solve the minimization of the target function (2). Firstly, given $\beta_{rc}^{(t)}$ and $S_{rc}^{(t)}$, we adopt the FISTA algorithm proposed in Beck & Teboulle (2009) to update $L^{(t+1)}$. Specifically, let $\tilde{Y}_{rc}^{(t)} = Y_{rc} - X_{rc}\beta_{rc}^{(t)} - M_{-rc}S_{rc}^{(t)}$,

$r = 1, \ldots, R; c = 1, \ldots, C$. Define

$$L^{(t+1)} = \arg\min_{L} \frac{1}{n} \sum_{r=1}^{R} \sum_{c=1}^{C} \left\| \tilde{Y}_{rc}^{(t)} - M_{rc} L_{rc} \right\|_F^2 + \lambda \|L\|_* = \arg\min_{L} \mathcal{L}^{(t)}(L) + \lambda \|L\|_*, \quad (3)$$

then $L^{(t+1)}$ is solved by a standard FISTA step, which combines a gradient descent method with a soft threshold on the nuclear norm of the estimator. Let $\tilde{L}^{(t)} = L^{(t)} + (r^{(t-1)} - 1)(L^{(t)} - L^{(t-1)})/r^{(t)}$, where $r^{(t)}$ is a scale parameter that is updated with the profiling procedure. The matrix soft threshold function is defined as, for any given matrix D and threshold δ,

$$\text{Soft}(D, \delta) = U_D^\top \text{diag}\left\{(\theta_i(D) - \delta)_+\right\} V_D, \quad (4)$$

where $D = U_D^\top \text{diag}\left\{\theta_i(D)\right\} V_D$ is the singular value decomposition of D. Then $L^{(t+1)}$ is updated according to

$$L^{(t+1)} = \text{Soft}\left(\tilde{L}^{(t)} - \nabla \mathcal{L}^{(t)}\left(\tilde{L}^{(t)}\right)/\eta, \lambda/\eta\right),$$

where $\nabla \mathcal{L}^{(t)}\left(\tilde{L}^{(t)}\right)$ is the derivative of the loss function $\mathcal{L}^{(t)}$ on point $\tilde{L}^{(t)}$ with $\mathcal{L}^{(t)}$ defined in (3). Since the treatments are taken from $\{-1, 1\}$, thus the updating rate *eta* is taken as $\eta = 2$ in our problem according to Beck & Teboulle (2009).

Secondly, X_{rc} is low dimensional and the target function is separable with respect to (r, c) given L. Given $L^{(t+1)}$ and $S_{rc}^{(t)}$, we apply the ordinary least square method to update $\beta_{rc}^{(t+1)}$. Denote $\bar{Y}_{rc}^{(t)} = Y_{rc} - M_{rc} L^{(t+1)} - M_{-rc} S_{rc}^{(t)}$ and estimate $\beta_{rc}^{(t+1)}$ by

$$\beta_{rc}^{(t+1)} = \arg\min_{\beta} \left\| \bar{Y}_{rc}^{(t)} - X_{rc}\beta_{rc} \right\|_F^2 / n.$$

Thirdly, given $L^{(t+1)}$ and $\beta_{rc}^{(t+1)}$, we solve $S_{rc}^{(t+1)}$ by the lasso method. Specifically, let $\dot{Y}_{rc}^{(t)} = Y_{rc} - X_{rc}\beta_{rc}^{(t+1)} - M_{rc} L_{rc}^{(t+1)}$ and we solve

$$S_{rc}^{(t+1)} = \arg\min_{S_{rc}} \frac{1}{n} \left\| \dot{Y}_{rc}^{(t)} - M_{-rc} S_{rc} \right\|_F^2 + \lambda_{rc} \|S_{rc}\|_1.$$

Finally, for a tolerance parameter τ, we end the estimation procedure if

$$\left\|\beta^{(t+1)} - \beta^{(t)}\right\|_F / \left\|\beta^{(t)}\right\|_F + \left\|L^{(t+1)} - L^{(t)}\right\|_F / \left\|L^{(t)}\right\|_F + \left\|S^{(t+1)} - S^{(t)}\right\|_F / \left\|S^{(t)}\right\|_F < \tau,$$

where $\beta = (\beta_{11}, \dots \beta_{RC}) \in \mathbb{R}^{d \times RC}$ and $S = (S_{11}, \dots S_{RC}) \in \mathbb{R}^{(RC-1) \times RC}$.

In the above procedure, the tuning parameter λ for the low-rank penalty can be selected by the 5-fold cross-validation. For the sparse tuning parameter λ_{rc}, we recommend to set $\lambda_{rc} = A\hat{\sigma}_{rc}\{\log(RC)/n\}^{1/2}$ with $A > 2\sqrt{2}$, where $\hat{\sigma}_{rc}$ is some consistent estimator of σ_{rc}. We summarize the estimation algorithm in Algorithm 1 as follows.

3.2 Global test

We consider the global testing problem for the interference matrix S in this subsection. The hypothesis of interest is

$$H_0 : S = 0 \quad \text{v.s.} \quad H_1 : S \neq 0. \tag{5}$$

When the null hypothesis is rejected, interference occurs across the space, and further detection of the specific locations of IE is required, as discussed in the next subsection. Otherwise, no interference is present. In this case, the post-detection outcome regression simplifies to an ordinary linear regression, allowing for efficient estimation and inference of the ATE.

Let $\hat{S}$ be the estimator of S under model (1). We propose to construct the test statistic based on the infinity norm of the normalized estimator (Zhang & Cheng 2017, Xue & Yao 2020). Specifically, for a matrix $A \in \mathbb{R}^{p_1 \times p_2}$, define $\|A\|_\infty = \max\{|A_{ij}| : i = 1, \dots, p_1; j = 1, \dots, p_2\}$. Then the test statistic is $T_n = \left\| \sqrt{n}\hat{S} \right\|_\infty$. This test will reject the null hypothesis at a certain significance level α if $T_n > c_B(\alpha)$ for some threshold $c_B(\alpha)$. The derivation of $c_B(\alpha)$ follows from a conditional bootstrap procedure. Specifically, let $\hat{\sigma}_{rc}$ be a consistent estimate of the noise levels σ_{rc}. We independently generate $e_{rc} = \{e_{irc}\}_{i=1}^n$ as a set of i.i.d. normal random variables from $\mathcal{N}(0, \hat{\sigma}_{rc}^2)$, $r = 1, \dots, R; c = 1, \dots, C$, respectively. Then let

$$Y_{rc}^e = (I - \mathcal{P}_{X_{rc}})e_{rc}, \ r = 1, \dots, R; \ c = 1, \dots, C,$$

Algorithm 1 Two-layer Profiling Algorithm

Input: observations $\{Y_{rc}, X_{rc}, M_{rc}, M_{-rc}\}_{r,c}$; tuning parameters $\lambda, \{\lambda_{rc}\}_{r,c}$; updating rate $\eta = 2$; scale parameters $r^{(-1)} = r^{(0)} = 1$; convergence tolerance τ; initial estimators $\beta^{(0)}, S^{(0)}$, $L^{(0)} = L^{(-1)}$.

Initialize $t \leftarrow 0$, $\delta^{(0)} \leftarrow 1$.

while $\delta^{(t)} \geq \tau$ **do**

  for $r = 1, \ldots, R,\ c = 1, \ldots, R$ **do**

    Compute $\tilde{Y}_{rc}^{(t)} \leftarrow Y_{rc} - X_{rc}\beta_{rc}^{(t)} - M_{-rc}S_{rc}^{(t)}$ and $\tilde{L}^{(t)} \leftarrow L^{(t)} + \frac{r^{(t-1)}-1}{r^{(t)}}\left(L^{(t)} - L^{(t-1)}\right)$;

    With Soft$(\cdot)$ and $\mathcal{L}^{(t)}$ defined in (4) and (3), respectively, update $L^{(t+1)} \leftarrow \text{Soft}\left(\tilde{L}^{(t)} - \Delta\mathcal{L}^{(t)}\left(\tilde{L}^{(t)}\right)/\eta, \lambda/\eta\right)$;

    Compute $\bar{Y}_{rc}^{(t)} \leftarrow Y_{rc} - M_{rc}L^{(t+1)} - M_{-rc}S_{rc}^{(t)}$ and update

$$\beta_{rc}^{(t+1)} \leftarrow \arg\min_{\beta} \left\|\bar{Y}_{rc}^{(t)} - X_{rc}\beta_{rc}\right\|_F^2 / n;$$

    Compute $\dot{Y}_{rc}^{(t)} \leftarrow Y_{rc} - X_{rc}\beta_{rc} - M_{rc}L_{rc}$ and update

$$S^{(t+1)} \leftarrow \arg\min_{S_{rc}} \frac{1}{n}\left\|\dot{Y}_{rc}^{(t)} - M_{-rc}S_{rc}\right\|_F^2 + \lambda_{rc}\left\|S_{rc}\right\|_1;$$

  end for

  Update $r^{(t+1)} \leftarrow \left\{1 + \sqrt{1 + 4\left(r^{(t)}\right)^2}\right\}/2$ and

$$\delta^{(t+1)} \leftarrow \frac{\left\|\beta^{(t+1)} - \beta^{(t)}\right\|_F}{\left\|\beta^{(t)}\right\|_F} + \frac{\left\|L^{(t+1)} - L^{(t)}\right\|_F}{\left\|L^{(t)}\right\|_F} + \frac{\left\|S^{(t+1)} - S^{(t)}\right\|_F}{\left\|S^{(t)}\right\|_F};$$

  $t \leftarrow t + 1$;

end while

Output: estimator $\hat{\beta} = \beta^{(t+1)}, \hat{L} = L^{(t+1)}$ and $\hat{S} = S^{(t+1)}$.

where $\mathcal{P}_{X_{rc}} = X_{rc}\left(X_{rc}^{\top}X_{rc}\right)^{-1}X_{rc}^{\top}$ is the projection matrix of X_{rc}. The rationale for constructing Y_{rc}^{e} in this manner is as follows. First, taking advantage of the low-rank assumption, the estimation error of DE is negligible compared to $\widehat{\beta}_{rc}-\beta_{rc}$, making it unnecessary to recompute L_{rc} in the bootstrap procedure. Second, it is worth noting that β_{rc} is estimated using the ordinary least square method. Given the convergence of profiling algorithms, it is equivalent to utilize $(I-\mathcal{P}Xrc)e_{rc}$ for estimating S_{rc} under the null hypothesis. Let $\hat{S}_{rc}^{e}$ be the lasso estimator of the optimization problem $\left\|Y_{rc}^{e}-M_{-rc}S_{rc}\right\|_{F}^{2}/n+\lambda_{rc}\left\|S_{rc}\right\|_{1}$ and $T_{n}^{e}=\left\|\sqrt{n}\hat{S}^{e}\right\|_{\infty}$. Then $c_{B}(\alpha)$ is calculated by

$$c_{B}(\alpha)=\inf\left\{t\in\mathbb{R}:\mathbb{P}_{e}\left(T_{n}^{e}\leq t\right)\geq 1-\alpha\right\},$$

where $\mathbb{P}_{e}\left(\cdot\right)$ denotes the probability measure with respect to $e=\{e_{rc}\}_{r,c=1}^{R,C}$. To approximate the critical value by the bootstrap, we generate N sets of normal random variables $e^{(1)},\ldots,e^{(N)}$ with each being a random copy of e. The corresponding estimates are denoted by $\hat{S}_{1}^{e},\ldots,\hat{S}_{N}^{e}$. While keeping the state and treatment fixed, we calculate N times of T_{n}^{e}, denoted as $\left\{T_{n}^{eb}:b=1,\ldots,N\right\}$ with $T_{n}^{eb}=\left\|\sqrt{n}\hat{S}_{b}^{e}\right\|_{\infty}$. Then we approximate $c_{B}(\alpha)$ by the $100(1-\alpha)$th sample percentile of $\left\{T_{n}^{eb}:b=1,\ldots,N\right\}$.

It remains to estimate the noise level σ_{rc} of each unit, $r=1,\ldots,R;c=1,\ldots,C$. Similar to Zhang & Cheng (2017), we adopt the scaled lasso in the high-dimensional linear model $Y_{rc}=Z_{rc}\gamma_{rc}+\varepsilon_{rc}$, where $Z_{rc}=(X_{rc},M_{rc},M_{-rc})$ and $\gamma_{rc}=\left(\beta_{rc}^{\top},L_{rc},S_{rc}^{\top}\right)^{\top}$. As discussed in Sun & Zhang (2012) and Sun & Zhang (2013), the universal penalty level $\rho=\{2\log(d+RC)/n\}^{1/2}$ generally has a good numerical performance.

3.3 Detection of interference

We now introduce how to detect the locations of interference, which is equivalent to identifying the locations of nonzero elements in the matrix $\hat{S}$. Although $\hat{S}$ is sparse, its nonzero elements still include many false signals (Zhao & Yu 2006). Hence we need to conduct a

further detection procedure on the matrix $\hat{S}$.

Denote $U_n = \left|\sqrt{n}\text{vec}(\hat{S})\right|$ and $U_n^{(b)} = \left|\sqrt{n}\text{vec}(\hat{S}^e_{(b)})\right|$, where $\text{vec}(\cdot)$ is the vectorization operator and $\hat{S}^e_{(b)}$ is the lasso estimator with respect to $e^{(b)}$ in the bootstrap procedure, $b = 1, \ldots, N$. Then the stepdown algorithm (Romano & Wolf 2005) can be applied to U_n, $U_n^{(1)}, \ldots, U_n^{(N)}$ to consistently detect the interference. Specifically, let $\eta_1 = \{1, \ldots, p\}$ at the first step where $p = RC(RC-1)$. Reject all hypotheses $H_{0,j}$ such that $U_{n,j} > c_B(\alpha; \eta_1)$, where the threshold $c_B(\alpha; \eta_l)$ is the empirical $1-\alpha$ quantile of $\left\|U_n^{(b)}(\eta_l)\right\|_\infty$ and $U_n^{(b)}(\eta_l)$ is the sub-vector which contains the elements with index in η_l. If no hypothesis is rejected, then stop. If some hypotheses are rejected, let η_2 be the set of indices for those hypotheses not being rejected at the first step. At step l, let $\eta_l \subset \eta_{l-1}$ be the subset of hypotheses that are not rejected at step $l-1$. Reject all hypotheses $H_{0,j}, j \in \eta_l$ satisfying that $U_j > c_B(\alpha; \eta_l)$. If no hypothesis is rejected, stop the algorithm. Denote the stopping point by l^*. Then the detected locations of interference is given by $\hat{J}_1 = \eta_1 \setminus \eta_{l^*}$, where "\" indicates the elements in η_1 but not in η_{l^*}.

An alternative method is the Binary and Re-Search (BiRS) algorithm proposed by Zhang et al. (2023). It involves a sequence of binary segmentation operations and dynamic tests to increase detection accuracy and reduce computation. The detection procedure is summarized as follows. At the first step, let $\eta_{1_1} = \{1, 2, \ldots, \lfloor p/2 \rfloor\}$ and $\eta_{1_2} = \{\lfloor p/2 \rfloor + 1, \ldots, p\}$ with $\lfloor \cdot \rfloor$ taking value of the largest integer below. The critical value is $c_B(\alpha; \eta_1)$ with $\eta_1 = \eta_{1_1} \cup \eta_{1_2}$. Let $T_{1_k} = \|U_n(\eta_{1_k})\|_\infty$ with $k = 1, 2$. If $T_{1_k} > c_B(\alpha; \eta_1)$, then η_{1_k} possibly contains IE and needs further detection by binary segmentation; otherwise, there is no interference within region η_{1_k}. For the l-th binary search, there exist $n(l)$ possible signal segments $\eta_{l_1}, \ldots, \eta_{l_{n(l)}}$, $1 \le n(l) \le 2^l$. For $k = 1, \ldots, n(l)$, when $T_{l_k} > c_B(\alpha; \eta_l)$, we take η_{l_k} as the set containing interference for the next search. The segmentation stops if $|\eta_{l_k}| = 1$. Denote the detected interference location set by $\hat{\eta}_1^{(0)}, \ldots, \hat{\eta}_{K_0}^{(0)}$. Let $\hat{\eta}^{(0)} = \cup_{k=1}^{K_0} \hat{\eta}_k^{(0)}$. In the re-search procedure, substitute the variables in $\hat{\eta}^{(0)}$ in $U_n, U_n^{(b)}, b = 1, \ldots, N$ with ze-

ros and repeat the global test and binary search. Add the newly detected locations to $\hat{\eta}^{(0)}$. Repeat the re-search procedure until the global test accepts that there is no interference and denote the final set of detected locations of interference by $\hat{J}_1$.

Based on the detection results, we can establish a "post-detection" estimator of ATE using the ordinary least square estimation in each unit if $s_{rc} \ll n$. Denote the detected locations of interference neighbors of unit (r, c) by $\hat{J}_1(r, c)$ and let $\hat{s}_{rc} = \#\hat{J}_1(r, c)$, $\tilde{Z}_{rc} = \left(X_{rc}, M_{rc}, M_{-rc,\hat{J}_1(r,c)}\right)$. For each unit (r, c), compute the $d + 1 + \hat{s}_{rc}$ dimensional ordinary least square estimator $\tilde{\gamma}_{rc} = \left(Z_{rc}^\top Z_{rc}\right)^{-1} Z_{rc}^\top Y_{rc}$. Then the post-detection estimator of ATE is given by

$$\hat{\text{ATE}} = \frac{2}{RC} \sum_{r=1}^{R} \sum_{c=1}^{C} \sum_{i=d+1}^{d+1+\hat{s}_{rc}} \tilde{\gamma}_{rci}, \tag{6}$$

where $\hat{s}_{rc} = \left|\hat{J}_1(r, c)\right|$. As $s_{rc} \ll RC$, the model dimension is substantially reduced as long as $\hat{J}_1(r, c)$ covers $J_1(r, c)$ with a high probability.

4 Theoretical Analysis

In this section, we present the non-asymptotic upper bound of the estimation error for the treatment effect coefficient estimates proposed in Section 3.1. Then we establish the theoretical guarantees of the global test under the null hypothesis in Section 4.2, and analyze the power of the global test and the accuracy of detection in Section 4.3.

4.1 Estimation error bound

We first impose the following assumptions on the random errors and treatment design.

Assumption 4 *For any fixed vector* $\delta \neq 0$, $2\left\|\mathcal{P}_{X_{rc}}\left(M_{rc}, M_{-rc}\right)\delta\right\|_2^2 < \left\|\left(M_{rc}, M_{-rc}\right)\delta\right\|_2^2$, *for* $r = 1, \ldots, R$; $c = 1, \ldots, C$.

Assumption 5 *For some integer s_{rc} such that $1 \leq s_{rc} \leq RC$, recall that $J_1(r,c)$ is the set of nonzero elements of the coefficient S_{rc} and $J_0(r,c)$ is the set of zero ones. Assume that the following condition holds: for any fixed $\delta \neq 0$ and $\left\|\delta_{J_0(r,c)}\right\|_1 \leq 3\left\|\delta_{J_1(r,c)}\right\|_1$,*

$$\kappa_{rc}(s_{rc}, 3) = \min_{|J_1(r,c)| \leq s_{rc}} \frac{\|M_{-rc}\delta\|_2}{\sqrt{n}\left\|\delta_{J_1(r,c)}\right\|} > 0.$$

Assumption 4 imposes certain restrictions on the algebraic correlation between the state and treatment. In simpler terms, to control the estimation error, the correlation between the state and treatment can not be too strong. This usually holds in experimental studies and is relatively easy to verify in observational studies. Based on these assumptions, we can derive the following results for the estimates of $\hat{L}$ and $\hat{S}$. Assumption 5 is the restricted eigenvalue (RE) condition, which is a classical assumption in lasso problem (Bühlmann & Van De Geer 2011, Bickel et al. 2009). For conciseness, in the following theorems, we only present the results for the low-rank case of $q = 0$ and further extension for the general case can be found in the proof of Theorem 1 in Supplementary Material.

Theorem 1 *Suppose that Assumption 4 holds, $L \in \mathcal{B}_0(v_0)$ and the regularization parameters $\lambda = 2\|\chi(M, \mathcal{P}, \varepsilon)\|_{\text{op}}/n$ and $\lambda_{rc} = A\sigma_{rc}\{\log(RC)/n\}^{1/2}$ with $A > 2\sqrt{2}$, where $\|\cdot\|_{\text{op}}$ is the operator norm for matrices and the (r,c)-element of $\chi(M, \mathcal{P}, \varepsilon)$ is $\varepsilon_{rc}^{\top}(I - \mathcal{P}_{X_{rc}})M_{rc}$. Then when $S = 0$, there exist constant K_1 such that*

$$\left\|\hat{L} - L\right\|_F \leq K_1 v_0^{1/2}\left\{(R+C)/n\right\}^{1/2},$$

holds with probability tending to one.

When $S \neq 0$ and $\|S_{rc}\|_0 = s_{rc}$, $r = 1, \ldots, R$; $c = 1, \ldots, C$, further assume that Assumption 5 holds, then with probability tending to one, we have

$$\left\|\hat{S} - S\right\|_F + \left\|\hat{L} - L\right\|_F \leq K_2 \max_{r,c} \sigma_{rc}\left\{s_{rc}RC\log(RC)/n\right\}^{1/2},$$

where $K_2 = 32A/\min_{r,c}\kappa_{rc}^2(s_{rc}, 3)$.

Theorem 1 establishes the upper bounds of estimation errors of regression coefficients, which lays the foundation of the following inference and detection analysis.

4.2 Size and power analysis for the global test

For the testing, we further assume the following assumption.

Assumption 6 *The limits* $\lim_{n\to\infty} M_{-rc}^{\top} M_{-rc}/n = H_{rc}$, $r = 1, \ldots, R$; $c = 1, \ldots, C$ *exist.*

Assumption 7 *For any* δ *satisfies that* $\|\delta\|_1 < K_2 \max_{r,c} \left[\sigma_{rc} \{s_{rc} \log(RC)/n\}^{1/2}\right]$, *we have* $\left\|\mathcal{P}_{X_{rc}} M_{-rc}\delta\right\|_\infty = o\left(n^{-1/2}\right)$.

Assumption 6 is commonly made for inference of lasso estimator, which implies that the treatments follow a stable strategy, which is easily satisfied in practice. Assumption 7 imposes a weaker correlation structure between the treatments and state variables compared to Assumption 4, in order to control the size of the global test. Then we have the following result.

Theorem 2 *Suppose that* $L \in \mathcal{B}_0(v_0)$ *and Assumption 1–7 hold. The regularization parameters* $\lambda = 2\left\|\chi(M, \mathcal{P}, \varepsilon)\right\|_{\text{op}}/n$ *and* $\lambda_{rc} = A\sigma_{rc}\{\log(RC)/n\}^{1/2}$ *with* $A > 2\sqrt{2}$. *Then under the null hypothesis, as* $n \to \infty$ *and* $\log^7\left(R^2C^2n\right)/n \to 0$, *then*

$$\mathbb{P}\left(T_n > c_B(\alpha)\right) \to \alpha$$

holds with probability tending to one.

This demonstrates the error bound between the reject probability of the proposed test and the size α under the null hypothesis. From Theorem 2, we can conclude that, under mild conditions, our testing method controls the size.

To assess the efficiency of our test, we also conduct a power analysis in this subsection. Denote the power of the global test by Power(T_n). Then we have the following theorem.

Theorem 3 *Under assumptions of Theorem 2 and suppose that the strength of the true interference satisfies* $\|S\|_\infty \geq 2K_2 \max_{r,c} \sigma_{rc} \{s_{rc} \log(R^2C^2n)/n\}^{1/2}$, *then as* $n \to \infty$ *and* $\log^7(R^2C^2n)/n \to 0$, *then*

$$\text{Power}(T_n) \geq 1 - 2n^{-2} \to 1$$

holds with probability tending to one.

Theorem 3 guarantees that the power of global test tends to 1 even if the effects are weak. To see this, the interference is sparse and $\max_{r,c} s_{rc} \lesssim \log(RC)$ holds generally. Then Theorem 3 only requires the signal strength to be $O(\log(RC)/\sqrt{n})$, which is fairly weak.

4.3 Detection accuracy

We next study the detection accuracy of the stepdown and BiRS algorithms. We introduce the Jaccard index to measure the similarity between two sets I_1 and I_2 as $\mathcal{J}(I_1, I_2) = |I_1 \cap I_2| / |I_1 \cup I_2|$. Let J_1 be the index set of nonzero elements in $\text{vec}(S)$. Recall that $\hat{J}_1$ is the detected index set of nonzero elements in $\text{vec}(S)$. Let $s = \sum_{r=1}^{R} \sum_{c=1}^{C} s_{rc}$ and recall that K_2 is the constant defined in Theorem 1. We impose the following assumptions to ensure consistent detection of the interference.

Assumption 8 *The strength of the true interference satisfies that*

$$\min\{|S_{J_1}|\} \geq 2K_2 \max_{r,c} \sigma_{rc} \left\{s_{rc} \log\left(R^2C^2n\right)/n\right\}^{1/2}.$$

Assumption 9 *For any* $(r,c) \neq (j,k)$, *as* $n \to \infty$: *(a)* $\left|M_{rc}^\top M_{jk}\right|/n \leq (K_2 \max_{r,c} \sigma_{rc} s_{rc})^{-1}$; *(b)* $\left|M_{rc}^\top M_{jk}\right|/n = o\left((\max_{r,c} \sigma_{rc} s_{rc})^{-1}\right)$.

Assumption 8 mandates that the interference strength is not too weak. Assumption 9 specifies the requirements on the correlation of treatments across regions to ensure the consistent detection of stepdown and BiRS algorithms, respectively, which can guide the

experimental design in practice. Let $\hat{J}_1^{\text{step}}$ and $\hat{J}_1^{\text{BiRS}}$ be the estimated interference set by stepdown and BiRS algorithms, respectively. Then we have the following theorem.

Theorem 4 *Suppose that assumptions of Theorem 2 hold. Under Assumptions 8 and 9(a), when* $n \to \infty$, $\log^7(R^2C^2n)/n \to 0$ *and* $s/\{RC/\log(RC)\}^{1/2} \to \infty$, *it holds that*

$$\mathbb{P}\left\{\mathcal{J}\left(J_1, \hat{J}_1^{step}\right) \to 1\right\} \to 1.$$

Under Assumptions 8 and 9(b) and , when $n \to \infty$, $\log^7(R^2C^2n)/n \to 0$ *and* $s \to \infty$, *it holds that*

$$\mathbb{P}\left\{\mathcal{J}\left(J_1, \hat{J}_1^{BiRS}\right) \to 1\right\} \to 1.$$

Theorem 4 indicates that the proposed method can consistently identify the interference neighbors of all units, ensuring reliable post-detection treatment effect inference. The detection accuracy requires the total interference count s to grow large, making this condition generally valid. Notably, even when this condition does not hold, coverage consistency is still guaranteed. Specifically, under Assumptions 1 – 8, when $n \to \infty$ and $\log^7(R^2C^2n)/n \to 0$, we have

$$\mathbb{P}\left(J_1 \subset \hat{J}_1^{step}\right) \to 1, \text{ and } \mathbb{P}\left(J_1 \subset \hat{J}_1^{BiRS}\right) \to 1.$$

We mention that, although the stepdown algorithm can accommodate a stronger correlation of treatments across regions, it tends to produce more conservative detection results than the BiRS algorithm, as evidenced in numerical experiments of Section 6. This is probably because the BiRS algorithm operates in shorter regions for detection and hence is empirically more efficient, especially when the signals are sparse. We recommend selecting the algorithm according to the situation at hand.

5 Case Study: Ride-Hailing Market Analysis

In this section, we apply the proposed method to the policy evaluation in the riding market. We utilize the same riding market simulator as in Zhou et al. (2021). The simulator accurately replicates the dynamic transitions of demand and supply, mimicking an actual on-demand ride-sourcing platform. The demand distribution is generated using historical data, while the driver supply distribution is initialized based on real data from the beginning of the day. The simulator's transition dynamics and order dispatching policies further refine the driver supply distribution. The simulated results closely align with real-world scenarios, with differences of less than 2% in important metrics such as drivers' revenue, response rate, and idle driver rate.

For our analysis, we utilize one month of simulated ride-hailing market data from Chengdu, the capital of Sichuan province in China. We focus on the geographic region spanning 30.52°N to 30.68°N and 104°E to 104.16°E, which we partition into a 10×10 grid of spatial units. The outcome variable of interest is the total income of drivers within each grid cell. State variables include the number of idle drivers and the number of ride requests. Treatments are assigned independently across regions and days, with equal probability (0.5) for a treatment value of 1 (representing incentive policies aimed at stimulating demand) or -1 (indicating no treatment or control).

The estimated interference structures at selected locations are visualized in Figure 2. The interference structure we observe exhibits an interesting pattern, where some locations experience interference effects from neighboring regions, while others are influenced by more distant areas. Most of the red dots in the three panels of Figure 2 mark the residential regions. In the left panel, the blue dot corresponds to a region with several popular tourist destinations, including Bailuwan Park. The blue dot in the middle panel represents the well-known New Century Global Center, and the blue dot in the right panel is located

near Huaxi Live Mall, a prominent entertainment hub. In all cases, the observed positive interference effects indicate that incentive policies targeting commercial centers, tourist attractions, and entertainment venues not only stimulate local demand but also generate spillover effects, influencing the drivers' incomes of residential regions located far away.

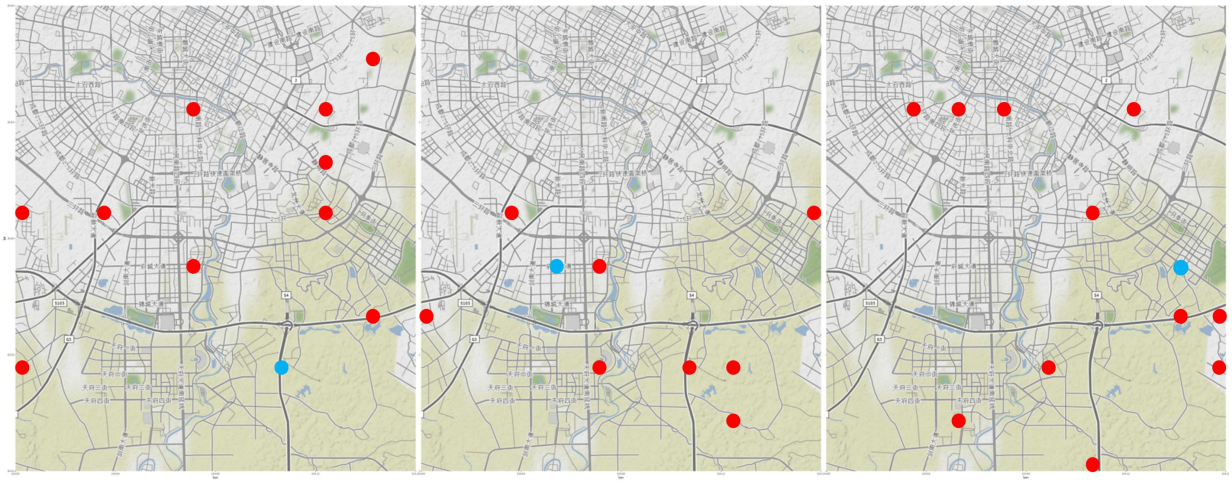

Figure 2: Interference structure of incentive policies on drivers' total income. In each panel, the regions marked with red dots represent areas where treatments (incentive policies) are applied, while the regions marked with blue dots indicate areas that experience spillover effects due to these treatments.

6 Real Data Based Simulations

To further evaluate the performance of the proposed method, we conduct comprehensive simulation studies inspired by real-world environmental scenarios. While our earlier example focused on the ride-hailing market, interference effects are also prevalent in environmental systems, where the impact of interventions often extends beyond targeted regions. For instance, the wind speed of one area can influence air quality in other regions due to atmospheric dispersion patterns. The data considered are the China meteorological forcing dataset (Jozsef Szilagyi 2019, Ma et al. 2019, Ma & Szilagyi 2019), download-

able at https://data.tpdc.ac.cn/en/data/8028b944-daaa-4511-8769-965612652c49. This is a gridded near-surface meteorological dataset with high spatial and temporal resolutions that was specifically developed for analyzing land surface processes in China. This dataset is created by merging remote sensing products, reanalysis datasets, and in-situ observation data from weather stations. It provides a continuous record starting from January 1979 and extending until December 2018, with a temporal resolution of three hours and a spatial resolution of 0.1°. The geographical coverage ranges from 70°E to 140°E and from 15°N to 55°N.

For our model, we select the 2-meter air temperature, surface pressure, specific humidity and 10-meter wind speed as the state covariates. The temperature is scaled to the unit $^{\circ}C$, while the pressure is scaled to the unit KPa. The sample size is $n = 100$, and the samples are randomly selected from daily data in 2018. Our analysis focuses on the center of Hebei province in China, where we divide the area of interest into $R \times C$ units, where $(R, C) = (12, 12)$ and $(16, 16)$ as two different configurations. For the area with dimensions of 12×12, the latitude spans from 37.85°N to 40.05°N with an interval of 0.2°, while the longitude spans from 114.85°E to 117.05°E with the same interval. In the case of the area with dimensions of 16×16, the latitude extends from 37.45°N to 40.45°N with an interval of 0.2°, and the longitude extends from 114.45°E to 117.45°E with the identical interval. We consider two scenarios for the design of treatments. The first one is the independent design, which randomly and independently assigns treatments in each unit with a probability of 1/2. This generates n treatment matrices $M_1, \ldots, M_n$. The second one is the correlated design. We independently generate random vectors $\tilde{M}_i$, where $i = 1, \ldots, n$, from a multivariate normal distribution $\mathcal{N}(0, \Sigma)$, where $\Sigma = \left(0.5^{|j-k|}\right)_{j,k=1}^{RC}$. These vectors are then transformed into matrices, and the treatment matrices M_i are generated by taking the sign of the corresponding vectors $\tilde{M}_i$.

To generate the matrix $M_{i,-rc}$, we employ the permutation operator $\mathcal{A}$. For $M_{i,-rc}$, the

application of $\mathcal{A}$ on $M_{i,-rc}$ orders the treatments of other locations based on the Euclidean distances to location (r, c). For illustrative purposes, consider a matrix $M = (m_{jk})_{j,k=1}^{3}$. The operation of $\mathcal{A}$ on M_{-11} is defined as follows:

$$M_{-11} = (m_{12}, m_{13}, m_{21}, m_{22}, m_{23}, m_{31}, m_{32}, m_{33})^{\top};$$

$$\mathcal{A}(M_{-11}) = (m_{12}, m_{21}, m_{22}, m_{13}, m_{31}, m_{23}, m_{32}, m_{33})^{\top}.$$

For generating regression coefficients, the state coefficient β is drawn from a standard normal distribution. The DE matrix L is generated based on the outcome matrix, conditioned on $M_{irc} = 0$. Specifically, let $F_{rc} = \sum_{i=1}^{n} X_{irc}\beta_{rc}/n$ for $r = 1, \ldots, R$ and $c = 1, \ldots, C$. Let

$$U_F^{\top} \mathrm{diag}\left\{\theta_i(F)\right\}_{i=1}^{n} V_F$$

be the singular value decomposition of F. Then, the DE matrix L is generated as

$$L = 0.01 \times U_F^{\top} \mathrm{diag}\left\{\theta_1, \theta_2, \theta_3, \theta_4, 0, \ldots, 0\right\} V_F.$$

The generated L exhibits a low-rank structure with a rank of 4, and its effect on the outcome Y is approximately 1%. In terms of the interference matrix S, for each unit (r, c), we randomly select $\eta_{rc} = \{0, 1, 2\}$ clusters of units that interfere with unit (r, c). Given unit (r, c), a cluster is defined as a set of units that have the same distance to unit (r, c). Additionally, given a strength parameter $\delta \in \{0, 2, 4, 6, 8, 10\} \times 10^{-3}$, the signal of nonzero IE is generated as ,

$$S_{rcj} \sim \delta \cdot TN(0, \infty, |F_{rc}|, 1), \quad j \in J_1(r, c),$$

where $TN(a, b, \mu, \sigma)$ is truncated normal distribution with support (a, b), mean μ and standard deviation σ. The tuning parameter λ for low-rank penalty is selected by 5-fold cross-validation and the sparse tuning parameter λ_{rc} is set to be $2\sqrt{3}\hat{\sigma}_{rc}\left\{\log(RC)/n\right\}^{1/2}$.

We begin by comparing the size of our testing method with that of the debiased lasso test under the null hypothesis ($\delta = 0$). To calculate the empirical sizes, we conduct 1000

Table 1: The empirical size of the proposed test and debiased lasso test in independent and correlated scenarios.

	$R \times C = 12 \times 12$		$R \times C = 16 \times 16$	
	Proposed	Debiased lasso test	Proposed	Debiased lasso test
Independent	0.0475	0.0725	0.0400	0.0325
Correlated	0.0525	0.0400	0.0500	0.0525

Monte Carlo simulations. Table 1 displays the results, showing that the proposed test effectively controls the size under both independent and correlated treatment designs with $(R, C) = (12, 12)$ and $(R, C) = (16, 16)$, while the size of debiased lasso test seems unstable in independent designs.

Next, we assess the detection accuracy by combining our testing method, debiased lasso test, with the BiRS and stepdown algorithms (referred to as Proposed-BiRS, Proposed-Step, debiased lasso-BiRS, and debiased lasso-Step, respectively). We compare their empirical false discovery rates and true positive rates. Additionally, we compare the popular Knockoff method under the low-rank and sparse effect model. The false discovery rates and true positive rates of each method are calculated with varying values of δ and (R, C), using 500 Monte Carlo simulations. The corresponding results are presented in Figure 3. In the independent treatment design, Proposed-BiRS exhibits the highest true positive rates and effectively controls the false discovery rates. Debiased lasso-BiRS has lower true positive rates than Proposed-BiRS, with a significant reduction in true positive rates when R, C increase. This is likely due to the fact that the debiased lasso method typically requires the design matrix to have a Gaussian distribution, and its performance is affected when a binary treatment design is used. The true positive rates and false discovery rates of the methods using the stepdown algorithm for detection are both lower than those using the BiRS algorithm, which supports the argument in Section 4. The Knockoff method

demonstrates the lowest overall detection accuracy. This is possibly because it is difficult to generate suitable knockoffs for a design matrix that only contains -1 and 1. In the correlated treatment design, when $(R, C) = (12, 12)$, the true positive rates of Proposed-BiRS are slightly inflated. These results indicate that the BiRS algorithm is preferred for less correlated treatment designs, while the stepdown algorithm can be applied to control the false discovery rates under more correlated designs.

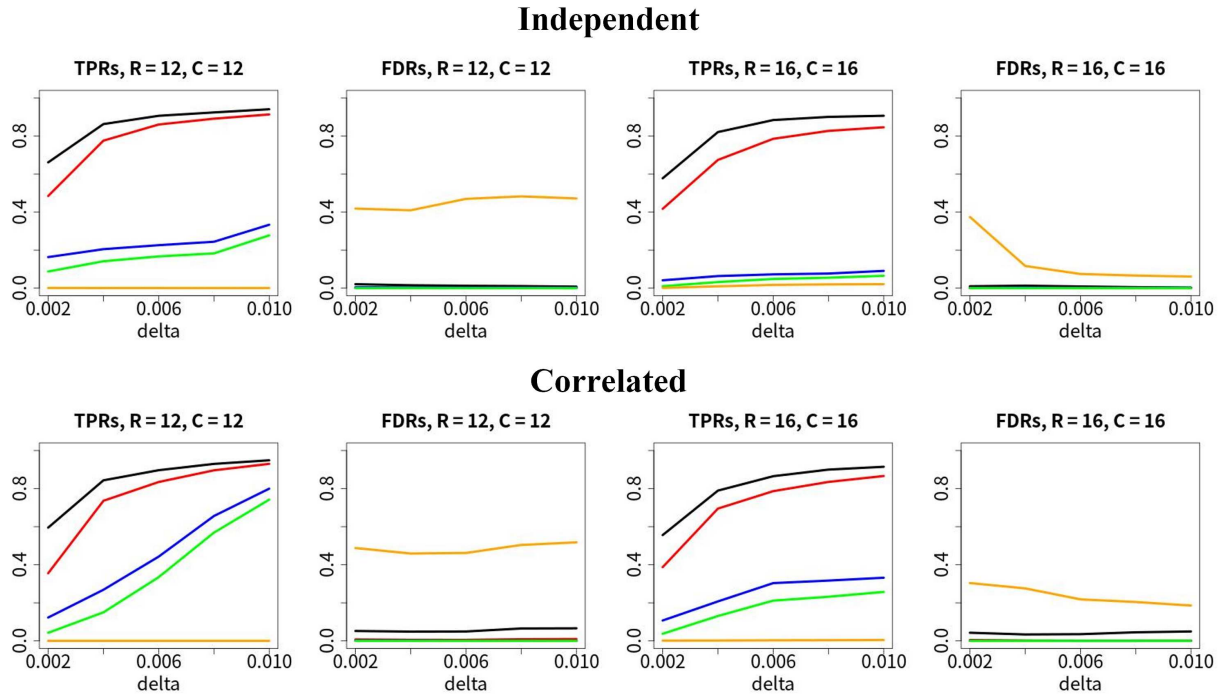

Figure 3: True positive rates (TPRs) and false discovery rates (FDRs) of various methods under the independent (the top row) and correlated (the bottom row) treatment design for different values of δ ($\delta = 0.002, 0.004, 0.006, 0.008$, and 0.010). In each row, the four panels correspond to true positive rates and false discovery rates when $(R, C) = (12, 12)$ and $(R, C) = (16, 16)$, respectively. In each panel, the proposed method with BiRS and stepdown algorithms are plotted in black and red lines, respectively. The debiased lasso with BiRS and stepdown algorithms are plotted in blue and green lines, respectively. The knockoff method corresponds to the orange lines.

Lastly, we compare the estimation performance of the post-detection ATE estimate with the ATE estimate computed using the mean field approximation. The mean field approximation assumes that the interference neighbors of each unit are regions that share a common edge with it, as discussed in Shi et al. (2022) and Hu et al. (2022). We calculate the empirical relative root mean square errors (RMSE) for both the post-detection ATE estimate and the mean field approximation ATE estimate across all previous settings, as depicted in the left two panels of Figure 4. This indicates that the mean field approximation fails to achieve satisfactory performance when the interference structure is mis-specified in contrast to the proposed method. We further investigate the relative RMSEs of the two estimates when the mean field assumption precisely holds. In this scenario, we define interference neighbors for each unit as those within a distance no greater than $2^{1/2}$. The results are presented in the right two panels of Figure 4. Here the mean field estimate serves as an oracle in this setting, and its RMSE can be regarded as the benchmark for the proposed estimate. Figure 4 clearly illustrates that the post-detection ATEs closely approximate the oracle ATE as the signal strengths improve. This demonstrates the effectiveness of the proposed method in a range of scenarios, regardless of whether the common edge assumption holds or not.

7 Discussion

In this work, we establish the framework for heterogeneous interference detection with theoretical guarantees. We introduce a low-rank and sparse model with a profiling algorithm, which is organically coupled with the high-dimensional signal detection method to identify the structure of spatial interference. We analyze the theoretical properties of the global test and detection procedure and demonstrate the effectiveness of our proposed method under mild assumptions.

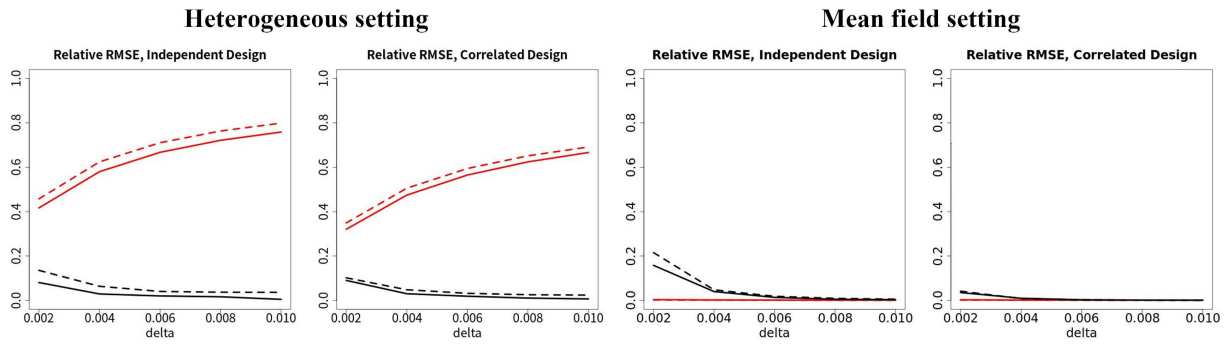

Figure 4: Relative RMSEs of ATE estimates under the independent and the correlated designs in the simulated heterogeneous interference setting (the left tow panels) and mean field interference setting (the right two panels). In each panel, the post-detection ATE estimate and the mean field approximation ATE estimate are plotted in black and red lines, respectively. The solid and dashed lines correspond to $(R, C) = (12, 12)$ and $(16, 16)$, respectively.

There are several important topics for future investigation. Firstly, we assume the noises $\{\varepsilon_{rc}\}_{r,c}$ are independent. It would be intriguing to explore the situation that the noises are spatially correlated. The main challenge lies in deriving an upper bound for the operator norm of element-correlated matrices in the low-rank estimation. One potential solution is to assume that the spatial dependence is local. Secondly, our focus in this work is on the parametric model. In the nonparametric setting, to address the curse of dimensionality, one may assume that the outcome of unit (r, c) is related to the state and treatment variables through either a sparse partially linear model (Xie & Huang 2009, Zhu et al. 2019), or a sparse single index model (Alquier & Biau 2013, Naik & Tsai 2001). Lastly, we discuss post-detection ATE estimation in this work and the inference of post-detection ATE can be an interesting topic for future studies.

SUPPLEMENTARY MATERIAL

TEM_supp Key lemmas, and proofs of the theoretical results for "High-dimensional De-

tection of Spatial Interference Effects". (.pdf file)

Acknowledgement

This research is supported by National Key Research and Development Program of China grants (No. 2022YFA1003800), the National Natural Science Foundation of China (No. 72301276, 12292981, 12288101), the New Cornerstone Science Foundation through Xplorer Prize, the Fundamental Research Funds for the Central Universities (LMEQF), an EPSRC grant EP/W014971/1, and the LMAM. We are grateful to Didichuxing for providing the data used in this study, which is essential to the completion of this research.

Disclosure Statement

The authors report there are no competing interests to declare.

References

Alquier, P. & Biau, G. (2013), 'Sparse single-index model.', *Journal of Machine Learning Research* **14**(1).

Altshuler, T., Altshuler, Y., Katoshevski, R. & Shiftan, Y. (2019), 'Modeling and prediction of ride-sharing utilization dynamics', *Journal of Advanced Transportation* **2019**(1), 6125798.

Aronow, P. M. & Samii, C. (2017), 'Estimating average causal effects under general interference, with application to a social network experiment', *The Annals of Applied Statistics* **11**(4), 1912–1947.

Arpino, B. & Mattei, A. (2016), 'Assessing the causal effects of financial aids to firms in tuscany allowing for interference', *The Annals of Applied Statistics* pp. 1170–1194.

Barkley, B. G., Hudgens, M. G., Clemens, J. D., Ali, M. & Emch, M. E. (2020), 'Causal inference from observational studies with clustered interference, with application to a cholera vaccine study', *The Annals of Applied Statistics* **14**(3), 1432–1448.

Beck, A. & Teboulle, M. (2009), 'A fast iterative shrinkage-thresholding algorithm for linear inverse problems', *SIAM journal on imaging sciences* **2**(1), 183–202.

Bickel, P. J., Ritov, Y. & Tsybakov, A. B. (2009), 'Simultaneous analysis of Lasso and Dantzig selector', *The Annals of Statistics* **37**(4), 1705–1732.

Bojinov, I. & Shephard, N. (2019), 'Time series experiments and causal estimands: exact randomization tests and trading', *Journal of the American Statistical Association* **114**(528), 1665–1682.

Bühlmann, P. & Van De Geer, S. (2011), *Statistics for high-dimensional data: methods, theory and applications*, Springer Science & Business Media.

Chernozhukov, V., Hansen, C., Liao, Y. & Zhu, Y. (2021), 'Inference for low-rank models', *arXiv preprint arXiv:2107.02602* .

Forastiere, L., Airoldi, E. M. & Mealli, F. (2021), 'Identification and estimation of treatment and interference effects in observational studies on networks', *Journal of the American Statistical Association* **116**(534), 901–918.

Giffin, A., Reich, B., Yang, S. & Rappold, A. (2020), 'Generalized propensity score approach to causal inference with spatial interference', *arXiv preprint arXiv:2007.0106* .

Goldsmith-Pinkham, P. & Imbens, G. (2013), 'Social networks and the identification of peer effects', *Journal of Business & Economic Statistics* **31**(1), 253–264.

Graham, B. S., Imbens, G. W. & Ridder, G. (2010), Measuring the effects of segregation in

the presence of social spillovers: a nonparametric approach, Technical report, National Bureau of Economic Research.

Halloran, M. E. (2012), 'The minicommunity design to assess indirect effects of vaccination', *Epidemiologic methods* **1**(1), 83–105.

Halloran, M. E. & Struchiner, C. J. (1991), 'Study designs for dependent happenings', *Epidemiology* pp. 331–338.

Halloran, M. E. & Struchiner, C. J. (1995), 'Causal inference in infectious diseases', *Epidemiology* pp. 142–151.

Hu, Y., Li, S. & Wager, S. (2022), 'Average direct and indirect causal effects under interference', *Biometrika* **109**(4), 1165–1172.

Hudgens, M. G. & Halloran, M. E. (2008), 'Toward causal inference with interference', *Journal of the American Statistical Association* **103**(482), 832–842.

Johari, R., Li, H., Liskovich, I. & Weintraub, G. Y. (2022), 'Experimental design in two-sided platforms: An analysis of bias', *Management Science* **68**(10), 7069–7089.

Jozsef Szilagyi, Liu Wenbin, Z. Y. (2019), 'Terrestrial evapotranspiration dataset across china (1982-2017)', *National Tibetan Plateau Data Center* .

Leung, M. P. (2022), 'Causal inference under approximate neighborhood interference', *Econometrica* **90**(1), 267–293.

Liu, L., Hudgens, M. G. & Becker-Dreps, S. (2016), 'On inverse probability-weighted estimators in the presence of interference', *Biometrika* **103**(4), 829–842.

Liu, T. L., Krishnakumari, P. & Cats, O. (2019), Exploring demand patterns of a ride-sourcing service using spatial and temporal clustering, *in* '2019 6th International Con-

ference on Models and Technologies for Intelligent Transportation Systems (MT-ITS)', pp. 1–9.

Luo, S., Yang, Y., Shi, C., Yao, F., Ye, J. & Zhu, H. (2024), 'Policy evaluation for temporal and/or spatial dependent experiments', *Journal of the Royal Statistical Society Series B: Statistical Methodology* **86**(3), 623–649.

Ma, N. & Szilagyi, J. (2019), 'The cr of evaporation: A calibration-free diagnostic and benchmarking tool for large-scale terrestrial evapotranspiration modeling', *Water Resources Research* **55**(8), 7246–7274.

Ma, N., Szilagyi, J., Zhang, Y. & Liu, W. (2019), 'Complementary-relationship-based modeling of terrestrial evapotranspiration across china during 1982–2012: Validations and spatiotemporal analyses', *Journal of Geophysical Research: Atmospheres* **124**(8), 4326–4351.

Munro, E., Wager, S. & Xu, K. (2021), 'Treatment effects in market equilibrium', *arXiv preprint arXiv:2109.11647* .

Naik, P. A. & Tsai, C.-L. (2001), 'Single-index model selections', *Biometrika* **88**(3), 821–832.

Papadogeorgou, G., Mealli, F. & Zigler, C. M. (2019*a*), 'Causal inference with interfering units for cluster and population level treatment allocation programs', *Biometrics* **75**(3), 778–787.

Papadogeorgou, G., Mealli, F. & Zigler, C. M. (2019*b*), 'Causal inference with interfering units for cluster and population level treatment allocation programs', *Biometrics* **75**(3), 778–787.

Perez-Heydrich, C., Hudgens, M. G., Halloran, M. E., Clemens, J. D., Ali, M. & Emch, M. E. (2014), 'Assessing effects of cholera vaccination in the presence of interference', *Biometrics* **70**(3), 731–741.

Romano, J. P. & Wolf, M. (2005), 'Exact and approximate stepdown methods for multiple hypothesis testing', *Journal of the American Statistical Association* **100**(469), 94–108.

Rubin, D. B. (1986), 'Comment: Which ifs have causal answers', *Journal of the American statistical association* **81**(396), 961–962.

Shi, C., Wan, R., Song, G., Luo, S., Song, R. & Zhu, H. (2022), 'A multi-agent reinforcement learning framework for off-policy evaluation in two-sided markets', *arXiv preprint arXiv:2202.10574* .

Sobel, M. E. (2006), 'What do randomized studies of housing mobility demonstrate? causal inference in the face of interference', *Journal of the American Statistical Association* **101**(476), 1398–1407.

Sun, T. & Zhang, C.-H. (2012), 'Scaled sparse linear regression', *Biometrika* **99**(4), 879–898.

Sun, T. & Zhang, C.-H. (2013), 'Sparse matrix inversion with scaled lasso', *The Journal of Machine Learning Research* **14**(1), 3385–3418.

Sävje, F., Aronow, P. & Hudgens, M. (2021), 'Average treatment effects in the presence of unknown interference', *Annals of statistics* **49**(2), 673.

Tchetgen, E. J., Fulcher, I. R. & Shpitser, I. (2021), 'Auto-g-computation of causal effects on a network', *Journal of the American Statistical Association* **116**(534), 833–844.

VanderWeele, T. J., Hong, G., Jones, S. M. & Brown, J. L. (2013), 'Mediation and spillover effects in group-randomized trials: a case study of the 4rs educational intervention', *Journal of the American Statistical Association* **108**(502), 469–482.

Wager, S. & Xu, K. (2021), 'Experimenting in equilibrium', *Management Science* **67**(11), 6694–6715.

Xie, H. & Huang, J. (2009), 'SCAD-penalized regression in high-dimensional partially linear models', *The Annals of Statistics* **37**(2), 673 – 696.

Xue, K. & Yao, F. (2020), 'Distribution and correlation-free two-sample test of high-dimensional means', *The Annals of Statistics* **48**(3), 1304 – 1328.

Zhang, W., Wang, F. & Yao, F. (2023), 'Binary and re-search signal region detection in high dimensions', *arXiv preprint arXiv:2305.08172* .

Zhang, X. & Cheng, G. (2017), 'Simultaneous inference for high-dimensional linear models', *Journal of the American Statistical Association* **112**(518), 757–768.

Zhang, Y., Loder, A., Rempe, F. & Bogenberger, K. (2022), 'Temporal aggregated analysis of gps trajectory data using two-fluid model', *Transportation Research Record: Journal of the Transportation Research Board* .

Zhao, P. & Yu, B. (2006), 'On model selection consistency of lasso', *Journal of Machine Learning Research* **7**(90), 2541–2563.

Zhou, F., Luo, S., Qie, X., Ye, J. & Zhu, H. (2021), 'Graph-based equilibrium metrics for dynamic supply–demand systems with applications to ride-sourcing platforms', *Journal of the American Statistical Association* **116**(536), 1688–1699.

Zhu, Y., Yu, Z. & Cheng, G. (2019), High dimensional inference in partially linear models, *in* 'The 22nd International Conference on Artificial Intelligence and Statistics', PMLR, pp. 2760–2769.